arXiv:1703.00614v1 [cond-mat.other] 2 Mar 2017

Nonlinear NMR signals and nuclear relaxation in coupled electron-nuclear spin systems

L. V. Abdurakhimov[1],* M. A. Borich[2,5], Yu. M. Bunkov[1,3,4], R. R. Gazizulin[3,4], D. Konstantinov[1],† M. I. Kurkin[2], and A. P. Tankeyev[2,5]

[1] *Okinawa Institute of Science and Technology (OIST) Graduate University, Onna, 904-0495 Okinawa, Japan*

[2] *Institute of Metal Physics, Ural Branch of Russian Academy of Sciences, 620990 Ekaterinburg, Russia*

[3] *CNRS Institute NEEL et Universite Grenoble Alpes, 38042 Grenoble, France*

[4] *Kazan Federal University, 420008 Kazan, Russia*

[5] *Ural Federal University, 620002 Ekaterinburg, Russia*

(Dated: March 3, 2017)

We present a new theoretical description of the coupled electron-nuclear spin systems which takes into account an indirect relaxation of nuclear spins via the electron subsystem. In our theory the magnitude of the nuclear magnetization is conserved for arbitrary large excitation powers, similar to the Landau-Lifshitz-Gilbert model of relaxation. This is drastically different from the conventional heating scenario based on the phenomenological Bloch equations. The predictions of our theory are compared with the experimental nonlinear NMR signals obtained in a weakly anisotropic antiferromagnetic $MnCO_3$ sample at temperatures below 1 K and good quantitative agreement is observed. The proposed theory brings together the properties of magnetic nuclear resonance in, on the one hand, the magnetic systems considered here and, on the other hand, the superfluid ^{3}He where the magnitude of the nuclear magnetization vector is also conserved.

PACS numbers: 75.45.+j, 75.30.Ds, 76.60.-k
Keywords: magnon BEC, non-linear NMR, $MnCO_3$

I. INTRODUCTION

A. Coupled electron-nuclear spin systems

Magnetically ordered spin systems with coupled electron-nuclear spin oscillations attracted general interest for a long time owing to their very peculiar nonlinear properties. In such systems the dynamics of the paramagnetic nuclear spin system is governed by the exceptionally strong (of the order 10^5-10^6 Oe) hyperfine field from the magnetically ordered electron spin system. In turn, the motion of electron spins is affected by the hyperfine field from the nuclear spins. This results in coupling between oscillations of electron and nuclear spin systems. From the microscopic point of view, one can describe such systems by pointing out that the coupled oscillations of the nuclear spins with the magnetically ordered electron subsystem introduce a long distance correlation between the precession of different nuclear spins.[1] This correlation can be described in terms of nuclear spin waves, i.e. n-magnons. From this point of view the hyperfine interaction leads to the hybridization of, on the one hand, usual spin waves in the magnetically ordered electron subsystem, i.e. e-magnons, and, on the other hand, the precession of a nuclear spin around the direction of the hyperfine field. Fig. 1 shows examples of spectra for hybridized e-magnons (frequency Ω_+) and n-magnons (frequency Ω_-) in a weakly anisotropic antiferromagnet $MnCO_3$. At zero wave number, $k = 0$, the frequency of n-magnons to a good approximation is given by

$$\Omega_-(0) \approx \omega_n - \omega_p, \tag{1}$$

where ω_n is the frequency of precession of the nuclear spin in stationary hyperfine field, that is when the oscillations of the electron spin system caused by coupling to the nuclear spins are neglected, and ω_p is a quantity that depends on a number of parameters including the temperature of the nuclear subsystem. At large k the spectrum of this branch approaches ω_n. Thus, the correlation between motion of different nuclear spins is significant only for small enough k, or in other words over a distance of typically 10^2-10^3 lattice sites. For the existence of n-magnons the frequency difference between $\Omega_-(0)$ and ω_n must satisfy the condition

$$\omega_n - \Omega_-(0) \gg \delta\omega_n, \tag{2}$$

where $\delta\omega_n$ is the spread in the frequency ω_n due to inhomogeneities of the atomic and magnetic structures of the sample (inhomogeneous broadening) and due to relaxation processes (homogeneous broadening). There are a few crystalline materials which satisfy this condition. Most notable examples are the weakly anisotropic antiferromagnets with ^{55}Mn as the magnetic ions, such as $MnCO_3$, $CsMnF_3$, $RbMnF_3$, $KMnF_3$, etc. The magnetic properties of these materials have been extensively studied by the continuous wave (CW) nuclear magnetic resonance (NMR),[2–7] double electron-nuclear magnetic resonance,[8–10] as well as pulsed NMR methods.[11–15]

An equivalent macroscopic description of coupled electron-nuclear spin systems is also possible.[16] Owing to correlated motion of a huge number (typically $\sim 10^{19}$) of spins, both the magnetically ordered electron spin subsystem and the paramagnetic nuclear spin subsystem can be described by a corresponding macroscopic net magnetization vectors **M** and **m**. The hyperfine interaction energy is given by $A\mathbf{Mm}$, where A

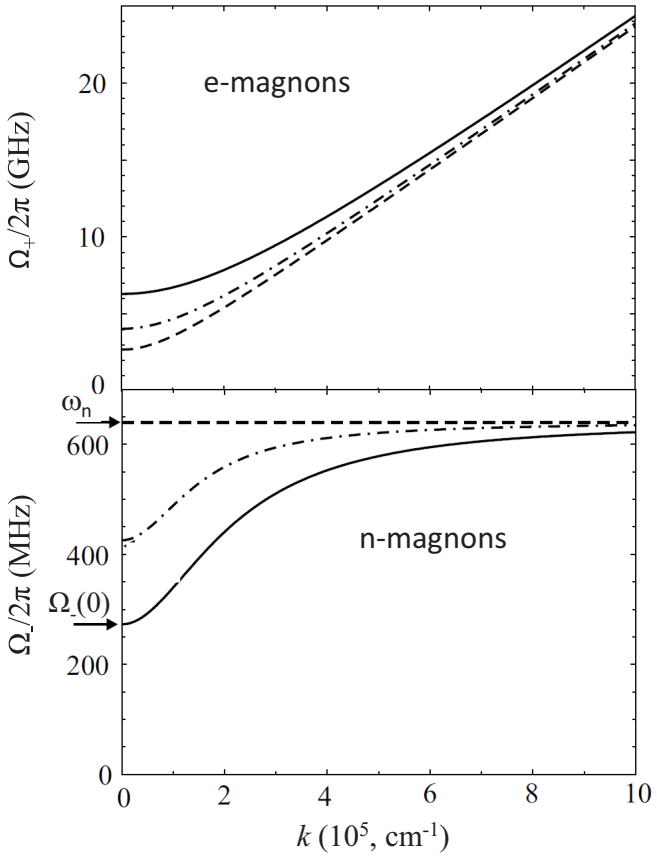

FIG. 1: The spectra of e-magnons and n-magnons in $MnCO_3$ in the static magnetic field of 0.2 kOe and at two values of temperature of 5 K (dashed-point line) and 1.4 K (solid line). The dashed lines show corresponding spectra in the case when coupling between electron and nuclear oscillations is neglected.

is the hyperfine interaction constant. Like for any two classical coupled oscillators, the spectrum of coupled precession of **M** and **m** vectors exhibit repulsion between the precession frequencies of two uncoupled spin subsystems. This results in two branches of a hybridized magnetic resonance, i.e. the quasi nuclear (q-NMR) and quasi electron (q-AFMR) modes of precession. The frequency of q-NMR mode is approximately given by

$$\omega_{\text{q-NMR}} \approx \omega_n - \omega_p \frac{m_z}{m_0}, \tag{3}$$

where $\omega_n = \gamma_n H_n$ ($H_n = A|\mathbf{M}|$ is the magnitude of the hyperfine field and γ_n is the gyromagnetic ratio of the nuclear spin), $m_0 = |\mathbf{m}|$ is the magnitude of the nuclear magnetization vector, and m_z is the magnitude of the projection of the vector **m** on the direction of stationary hyperfine field $\mathbf{H_n} \| \mathbf{z}$. The last term in Eq. (3) is usually referred to as the dynamical frequency shift, or frequency pulling. Note that for $m_z \approx m_0$, that is for negligible deflection of the nuclear magnetization vector from the equilibrium position, the frequency of q-NMR mode approaches the bottom of the n-magnon spectrum, see Eq. (1). From the equivalent microscopic point of view, the magnetization deflection may be described by a density of non-equilibrium magnons excited by a pulsed or CW radio-frequency (rf) pumping. We note that the frequency of q-AFMR mode decreases with the increase of the density of non-equilibrium magnons. This means that the e-magnons have an attractive interaction and the homogeneous precession is unstable. In contrast, the frequency of q-NMR mode increases with deflection of nuclear magnetization from equilibrium. This shows the repulsive interaction between n-magnons and leads to stability of the homogeneous precession.

Since the n-magnons obey Bose-Einstein statistics, there arises an important question about whether the non-equilibrium magnons can form a Bose-Einstein condensate (BEC) at rf pumping that creates a sufficiently large density of non-equilibrium magnons.

B. The BEC of non-equilibrium magnons

The peculiar non-linear properties described above are very similar to magnetic properties of the superfluid phase of ^{3}He. Therefore, in this section we would like to review main experimental findings in this system, in particular the formation of a BEC of non-equilibrium magnons. The first study of nonlinear magnetic resonance in superfluid ^{3}He was performed at the Kapitza Institute in Moscow and revealed a long lived induction decay signal after a pulsed NMR pumping in ^{3}He-B.[18] This signal was explained as a formation of a domain with a homogeneously precessing nuclear magnetization.[19] This state corresponds to the phase-coherent precession of magnetization even in a strongly inhomogeneous static magnetic field and corresponds to the global minimum of the Ginzburg-Landau potential for a non-equilibrium magnon system. Later, this state was associated with the formation of magnon BEC, and it is possible to show a close analogy between the formation of atomic BEC and magnon BEC.[20]

More recently, another type of magnon BEC was observed in thin films of yttrium iron garnet ($Y_3Fe_5O_{12}$) in a static magnetic field applied along the plane of the film.[21,22] In this case the minimum of the global energy corresponds to the spin waves with the wave numbers $k \sim 10^5\,\text{cm}^{-1}$. This magnon BEC state corresponds to a high-amplitude interference pattern of stationary spin waves with wave vectors **k** and $-\mathbf{k}$, and has some similarities with the charge density waves in superconductors. We will not consider this type of magnon BEC here.

The condition for magnon BEC formation follows directly from Bose-Einstein statistics according to which the occupation number for the magnon state with the wave number k is given by

$$n_k = \left[\exp\left(\frac{\hbar\Omega_-(k) - \mu}{k_B T}\right) - 1\right]^{-1}, \tag{4}$$

where μ is the chemical potential and T is the effective temperature of the nuclear system. As usual, the condition for the formation of a BEC with $k = 0$ corresponds to $n_0 \to \infty$. The

atomic BEC forms when the temperature of an atomic system decreases below the critical temperature T_c at which $\mu = 0$. In the case of a magnon system, for which μ is always zero in thermal equilibrium, one needs to create non-equilibrium magnons by external rf pumping to increase their chemical potential. Correspondingly, at a given temperature T the BEC is formed when condition $\hbar\Omega_-(0) = \mu$ is reached. The critical density N_c of the magnons which satisfy the above condition can be written as[23]

$$N_c = \frac{N_T \omega_n}{\omega_n - \Omega_-(0)}, \tag{5}$$

where N_T is the density of thermal magnons at a given temperature T. The critical density of magnons is related to the angle β of deflection of the macroscopic nuclear magnetization vector from its equilibrium orientation as $N_c = N_0(1-\cos\beta)$, where N_0 is roughly the number of the nuclear spins in a sample. Since typically $N_0 \sim 10^{19}$, the critical angle $\beta_{\rm BEC}$ needed to reach BEC can be as low as a few degrees.[23] The next question is the stability of non-equilibrium magnons. If homogeneous precession is not stable, the thermalization of the magnon system leads to the increase of the temperature of magnetic system and the critical density of magnons given by Eq. (5) increases. However, if coherent precession of magnons is supported by the minimum of the magnetic energy potential, then the magnons form the BEC which lives a relatively long time. Thus, the stability of homogeneous precession of nuclear magnetization is the crucial point in the formation of BEC.

Next, let us discuss the fundamental difference between magnon BEC state and usual magnetic resonance in magnetically-ordered media. Usually in the analysis of magnetic resonance in a sample, we must take into account the inhomogeneous broadening of the NMR line. The magnetic resonance signal is formed by a set of relatively independent magnetic oscillators which have different local frequencies. In the case of magnetically-ordered media the correlation between these oscillators appears on the distances of the effective magnetic interactions, i. e. 10-10^4 interatomic distances. In the magnetically-ordered media considered above, the precession frequency depends on the deflection angle of the magnetization, therefore on the density of pumped non-equilibrium magnons and interaction between them. This interaction can be attractive or repulsive. In the first case, the well-known effects of instability in atomic BEC[24] and magnon BEC[25] take place. We are interested in the second case when it is energetically favorable to conserve the homogeneity of precession. When the density of non-equilibrium magnons reaches the critical value, they form condensate described by a single macroscopic wave function. The magnons in BEC precess with the same frequency and with a small spreading of the phase which compensates for the inhomogeneity of the external conditions. In the BEC state, the transverse component of magnetization is described by a wave function $M_\perp \exp(i(\omega t + \phi))$, where $M_\perp$ is the magnitude of the projection of the magnetization vector on the plane perpendicular to the stationary hyperfine field and ϕ is the phase of the wave function at $t = 0$. This wave function describes all properties of the spin superfluidity.

The best system for investigation of magnon BEC and spin superfluidity is superfluid ^{3}He-B. In this system, there were found many phenomena which have one to one correspondence with the analogous phenomena of mass superfluidity and superconductivity. For example, critical supercurrent and phase slippage[26], the Josephson spin-current effect[27], as well as spin-current vortices[28] and Goldstone modes[29–31], were found. During the last 30 years, five different magnon BEC states were found in the ^{3}He superfluids. Comprehensive reviews can be found in the literature[32–37].

Unlike ^{3}He-B, the A-phase of superfluid ^{3}He has a different magnetic properties. The superfluid ^{3}He-A is an easy-plane two sublattice liquid antiferromagnet, which magnetic properties are described by a classical antiferromagnetic Hamiltonian. Homogeneous precession of the magnetization in bulk ^{3}He-A is not stable due to the attractive interaction between the magnons. Such an instability was predicted theoretically[38] and also observed experimentally[39,40]. Later it was suggested by Bunkov and Volovik[25] that a reorientation of the orbital momentum of ^{3}He-A could lead to a repulsive interaction between the magnons and to their BEC formation. This suggestion was confirmed in experiments with ^{3}He-A immersed in aerogel which had been squeezed along the magnetic field. In this case, aerogel orients the orbital momentum of ^{3}He-A along the magnetic field.[41,42] In such a configuration the magnon BEC was observed.[43,44]

The observation of magnon BEC in ^{3}He-A is important for the subject of this paper because the dynamic properties of NMR in antiferromagnets, as discussed here, are similar to the dynamic magnetic properties of superfluid ^{3}He-A in squeezed aerogel. The magnon BEC in the system with Suhl-Nakamura interaction was predicted[45] and subsequently found in $CsMnF_3$ and $MnCO_3$.[46,47] This observation sparked a discussion about magnon BEC in solid magnets. The main objection was related to the question of magnetic relaxation. It is customary to describe the nuclear magnetic relaxation by the phenomenological Bloch equations according to which the deflected magnetization must thermalize on a time scale T_2. However, pulsed NMR experiments showed the formation of a relatively long lived induction decay signal, similar to one observed in the superfluid ^{3}He-A.[48] This indicates that the nuclear magnetization is not described by the Bloch equations. In particular, the magnitude of the magnetization vector does not change under magnetization deflection and relaxation. This article provides detailed theory and experimental confirmation of this effect. In Section II, we provide a full macroscopic description of coupled electron-nuclear spin systems based on the Landau-Lifshiz-Gilbert equations linearized with respect to the transverse components of the electron magnetization vector. In Section III we describe measurements of the nonlinear NMR signals in a weakly anisotropic easy-plane antiferromagnet $MnCO_3$ and provide detailed comparison with our theory. Some details for the derivation of the coupled Landau-Lifshiz-Gilbert equations are given in the Appendix.

II. THEORETICAL DESCRIPTION

A. BEC formation in non-equilibrium n-magnons: qualitative microscopic analysis

It is convenient to start with the expression for spectrum of coupled electron-nuclear spin waves.[49] In the case of the weakly anisotropic antiferromagnets, the spectrum is given by (see Fig. 1)

$$\Omega_{\pm}^2(k) = \frac{1}{2}\left(\omega_e^2(k) + \omega_\Delta^2 + \omega_n^2\right) \pm \\ \pm \frac{1}{2}\left[\left(\omega_e^2(k) + \omega_\Delta^2 + \omega_n^2\right)^2 - 4\omega_e^2(k)\,\omega_n^2\right]^{1/2}. \quad (6)$$

In the above equation, the frequency $\omega_e(k)$ of a low-frequency branch of electron spin waves obtained by ignoring the hyperfine interaction of electrons with nuclei is given by

$$\omega_e^2(k) = \gamma_e^2 H(H + H_D) + \gamma_e^2 H_E^2 (ak)^2, \quad (7)$$

where γ_e is the gyromagnetic ratio of the electron spin, $a \approx 3\times 10^{-8}$ cm is the inter-atomic distance, and the exchange (H_E) and Dzyalushinskii-Moriya (H_D) effective magnetic fields will be defined in the next section. We also use notation

$$\omega_\Delta^2 = \gamma_e^2 H_E H_n \frac{m_0}{M_0} \quad (8)$$

where M_0 and m_0 are the magnitudes of the electron and nuclear magnetization vectors. It describes the gap in the spectrum of the e-magnon branch $\Omega_+^2(k)$ at H=0 (the so called hyperfine gap). This value can be considered as a measure of influence of the nuclear spins on the electron spin oscillations. In particular, the critical value of external magnetic field $H = H_c$ defined by

$$H_c(H_c + H_D) = H_E H_n \frac{m_0}{M_0}, \quad (9)$$

separates the regions of weak ($H > H_c$) and strong ($H < H_c$) influence of nuclear spins on the dynamics of the electron spins. For $MnCO_3$, we have $H_c \approx 0.7$ kOe at $T \approx 1$ K.

The $k = 0$ mode of n-magnon branch $\Omega_-(k)$ corresponds to the homogeneous precession of nuclear spins and is usually excited by the homogeneous rf magnetic field at the frequency $\omega = \Omega_-(0) \equiv \omega_{\text{q-NMR}}$. An important feature of the resonance frequency $\omega_{\text{q-NMR}}$ is its dependence on the projection of nuclear magnetization vector $\mathbf{m}$ on the direction of the hyperfine field $\mathbf{H_n}\|\mathbf{z}$, see Eq. (3). This prevents us from obtaining large deflection angles $\beta = \arccos(m_z/m)$ by the rf excitation at the resonance frequency ω given above. The reason for this is the deviation from the resonance condition $\omega = \omega_{\text{q-NMR}} = \omega_n - \omega_p \cos\beta$ at increasing β. However, it is possible to overcome this restriction by using the rf pumping at frequency in the interval $\omega_n - \omega_p < \omega < \omega_n$. Such rf pumping does not excite the homogeneous precession of $\mathbf{m}$, that is $k = 0$ mode of n-magnons, if the frequency detuning satisfies the condition $\Delta\omega = (\omega - \omega_n + \omega_p) >> \gamma_n H_1$, where H_1 is the amplitude of the rf magnetic field. On the other hand, in the frequency band of n-magnons there is a wave vector $k \neq 0$ such that $\Omega_-(k) = \omega$, see Fig. 2. The momentum conservation prohibits direct resonant excitation of such magnons by the homogeneous rf pumping. However, their indirect excitation is possible through intermediaries which are able to bypass the requirements of the momentum conservation, as was suggested earlier.[47] The analysis showed that the appearance of such n-magnons decreases the energy of nuclear spin system, therefore further leads to their gradual accumulation. In turn, the accumulation of n-magnons will lead to the increase of the defection angle and modification of the frequency band $\omega_+(k)$ of n-magnons. As a result, the n-magnons with frequency $\Omega_-(k)$ for given $k \neq 0$ become out of resonance with the rf pumping. The further evolution of such non-resonant n-magnons can proceed according to two possible scenarios. The first one corresponds to their thermalization, which increases the temperature of the nuclear spin system, i.e. the heating scenario. The heating of the nuclear subsystem decreases the magnitude of the magnetization vector $\mathbf{m}$. The nuclear temperature increases until the bottom of the n-magnon spectrum reaches the rf pumping frequency, that is $\omega_n - \omega_p' = \omega$, where ω_p' corresponds to the new temperature of the nuclear subsystem. The stationary state is characterized by a small amplitude of homogeneous precession of $\mathbf{m}$ having a significantly smaller magnitude.

In another scenario, two n-magnons with wave vectors $\pm\mathbf{k}$ can mutually transform their $|\mathbf{k}|$ to the value $|\mathbf{k} - \delta\mathbf{k}|$ which corresponds to the new resonance condition $\Omega_-(|\mathbf{k} - \delta\mathbf{k}|) = \omega$. Thus, the rf pumping and accumulation of magnons continues, leading to further increase of deflection angle β, and so on. The accumulation of magnons and increasing of deflection angle stops when the bottom of the frequency band of n-magnons reaches the rf pumping frequency

$$\omega_n - \omega_p \cos\beta_0 = \omega, \quad (10)$$

see dash-dotted line in Fig. 2. In this scenario, all accumulated n-magnons which provide the value of the deflection angle in the above equation are transformed into n-magnons with $k = 0$, which form a BEC with anomalously large magnon density.

In the next section we provide the quantitative macroscopic description of the steady states for both scenarios. The scenario with heating corresponds to the Bloch relaxation model which is described by the phenomenological longitudinal and transverse relaxation times. The scenario with deflection of magnetization vector $\mathbf{m}$ which conserves the vector magnitude corresponds to the indirect relaxation of n-magnons via the electron spin systems. This mechanism appears as a consequence of the coupled oscillations of $\mathbf{M}$ and $\mathbf{m}$ magnetization vectors. The preliminary results of this theoretical description were discussed earlier.[50]

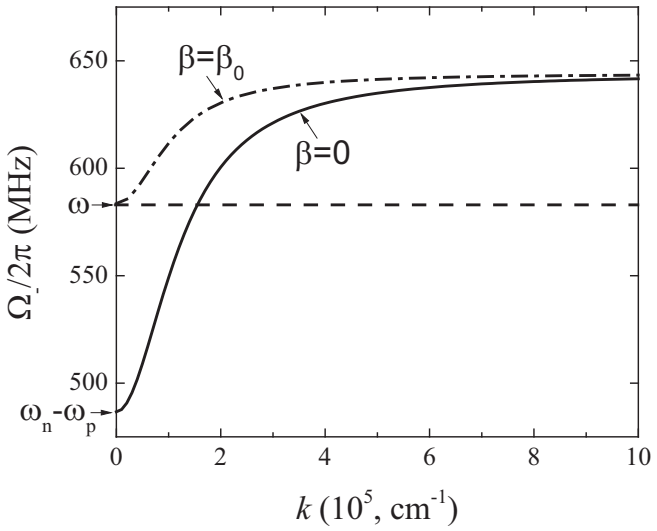

FIG. 2: The spectrum of n-magnons in $MnCO_3$ for zero deflection angle (solid line) and for deflection angle given by Eq. (10) (dash-dotted line). The frequency of rf pumping ω is indicated by a dashed line.

B. Macroscopic description of coupled electron-nuclear spin oscillations

Our theoretical analysis of a coupled electron-nuclear spin system in the easy-plane antiferromagnet $MnCO_3$ is based on the classical Landau-Lifshitz-Gilbert equations for macroscopic magnetization vectors of magnetic sub-lattices.[51–55] As usual, such an analysis of quantum spin systems is justified because the quantum-mechanical equations of motion reduce to the classical equations for the precession of the macroscopic magnetization vectors after averaging over the quantum-mechanical density matrix operator. Following the previous work,[49] we describe the dynamics of coupled electron-nuclear spin system by equations for two electron ($\mathbf{M}_1$ and $\mathbf{M}_2$) and two nuclear ($\mathbf{m}_1$ and $\mathbf{m}_2$) magnetization vectors of two sub-lattices

$$\begin{aligned}\frac{\mathrm{d}\mathbf{M}_1}{\mathrm{d}t} &= \gamma_e\left(\mathbf{M}_1\times\mathbf{H}_{\mathrm{M}_1}\right)+\mathbf{R}_{\mathrm{M}_1},\\ \frac{\mathrm{d}\mathbf{M}_2}{\mathrm{d}t} &= \gamma_e\left(\mathbf{M}_2\times\mathbf{H}_{\mathrm{M}_2}\right)+\mathbf{R}_{\mathrm{M}_2},\end{aligned}\tag{11}$$

$$\begin{aligned}\frac{\mathrm{d}\mathbf{m}_1}{\mathrm{d}t} &= \gamma_n\left(\mathbf{m}_1\times\mathbf{H}_{\mathrm{m}_1}\right)+\mathbf{R}_{\mathrm{m}_1},\\ \frac{\mathrm{d}\mathbf{m}_2}{\mathrm{d}t} &= \gamma_n\left(\mathbf{m}_2\times\mathbf{H}_{\mathrm{m}_2}\right)+\mathbf{R}_{\mathrm{m}_2},\end{aligned}\tag{12}$$

where $\mathbf{H}_{\mathrm{M}_1}$ and $\mathbf{H}_{\mathrm{M}_2}$ ($\mathbf{H}_{\mathrm{m}_1}$ and $\mathbf{H}_{\mathrm{m}_2}$) are the effective magnetic fields acting on each electron (nuclear) sub-lattice, and $\mathbf{R}_{\mathrm{M}_1}$ and $\mathbf{R}_{\mathrm{M}_2}$ ($\mathbf{R}_{\mathrm{m}_1}$ and $\mathbf{R}_{\mathrm{m}_2}$) are the relaxation terms for the electron (nuclear) magnetization in each sub-lattice. The effective magnetic fields are given by

$$\mathbf{H}_{\mathrm{M_i}}=-\frac{\partial\Phi}{\partial\mathbf{M}_i},\quad \mathbf{H}_{\mathrm{m_i}}=-\frac{\partial\Phi}{\partial\mathbf{m}_i},\quad i=1,2.\tag{13}$$

The thermodynamic potential of the whole spin system including its interaction with the external static and rf magnetic fields is given by

$$\Phi=\Phi_{ex}+\Phi_A+\Phi_D+\Phi_H+\Phi_{hyp}.\tag{14}$$

The exchange interaction between electron spins of the two sub-lattices is described by

$$\Phi_{ex}=\frac{1}{V}\int d\mathbf{r}\int d\mathbf{r}' J\left(r-r'\right)\mathbf{M}_1\left(r\right)\mathbf{M}_2\left(r'\right),\tag{15}$$

where $J>0$ describes the exchange interaction and V is the sample volume. The energy of magnetic anisotropy with dedicated axis $\mathbf{c}$ chosen as the positive $\mathbf{y}$ direction is described by

$$\Phi_A=\frac{1}{V}\int d\mathbf{r}K\left[\left(M_1^y\left(r\right)\right)^2+\left(M_2^y\left(r\right)\right)^2\right].\tag{16}$$

In the antiferromagnet $MnCO_3$ considered here, this anisotropy is the easy-plane which corresponds to the condition $K>0$. The Dzyaloshinskii-Moriya interaction which is responsible for non-collinearity of the $\mathbf{M}_1$ and $\mathbf{M}_2$ sublattices, see Fig. 3, is described by

$$\Phi_D=\frac{1}{V}\int d\mathbf{r}D\left(M_1^x\left(r\right)M_2^z\left(r\right)-M_1^z\left(r\right)M_2^x\left(r\right)\right).\tag{17}$$

where D is a constant which characterizes the strength of Dzyaloshinkii-Moriya interaction. The energy of $\mathbf{M}_1$ and $\mathbf{M}_2$ magnetizations in the external static magnetic field $\mathbf{H}$ applied in the positive $\mathbf{x}$ direction and ac magnetic field $\mathbf{h}(t)$ applied along axis z is described by

$$\begin{aligned}\Phi_H=&-\frac{1}{V}\int d\mathbf{r}H\left(M_1^x\left(r\right)+M_2^x\left(r\right)\right)-\\ &-\frac{1}{V}\int d\mathbf{r}h\left(t\right)\left(M_1^z\left(r\right)+M_2^z\left(r\right)\right).\end{aligned}\tag{18}$$

In what follows, we neglect direct interaction of nuclear magnetization vectors $\mathbf{m_1}$ and $\mathbf{m_2}$ with the static and rf magnetic fields compared to the much stronger hyperfine field. However, note that the rf magnetic field still strongly couples to the nuclear spins via the $\mathbf{h}(t)$-induced oscillations of the electron magnetization. The hyperfine interaction between the electron and nuclear spins, which for simplicity we assume to be isotropic, is described by

$$\Phi_{hyp}=-\frac{1}{V}\int d\mathbf{r}A\left(\mathbf{M}_1\left(r\right)\mathbf{m}_1\left(r\right)+\mathbf{M}_2\left(r\right)\mathbf{m}_2\left(r\right)\right).\tag{19}$$

At $\mathbf{h}(t)$=0, the condition of minimum of the functional (14) defines the equilibrium orientation of the vectors $\mathbf{M}_{1,2}$ and $\mathbf{m}_{1,2}$, see Fig. 3. The small angle ψ in this figure is determined from the equation

$$\sin\psi = \frac{H+H_D}{H_E}, \tag{20}$$

where $H_D = DM_0$ is the magnitude of the Dzyaloshinskii-Moria field, $M_0 = |\mathbf{M}_1| = |\mathbf{M}_2|$ is the magnitude of the electron magnetization vector in each sub-lattice, and the exchange field is given by

$$H_E = 2M_0^{-1}\int d\left(\mathbf{r}-\mathbf{r}'\right) J\left(\mathbf{r}-\mathbf{r}'\right) \tag{21}$$

The typical angle ψ is of the order 10^{-2} rad

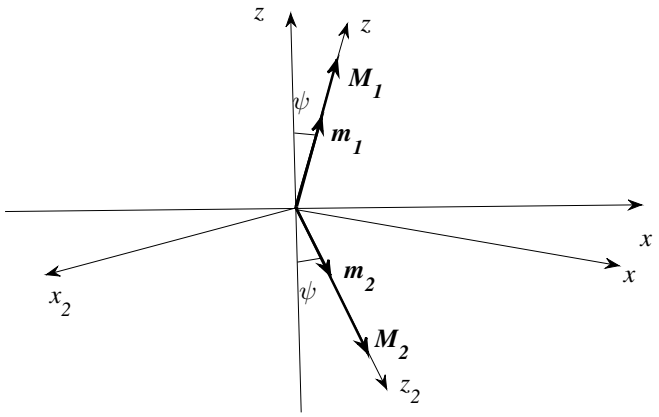

FIG. 3: Equilibrium position of the electron and nuclear magnetization vectors for each sub-lattice.

The solutions of Eqs. (11-19) for the small deviations of $\mathbf{M}_{1,2}$ and $\mathbf{m}_{1,2}$ from their equilibrium orientations were investigated earlier.[16,49] In this case, the eigenmodes of coupled electron-nuclear oscillations can be found from Eqs. (11-12) linearized with respect to the transverse components of magnetization vectors $\mathbf{M}_{1,2}$ and $\mathbf{m}_{1,2}$ and by taking the rf field $\mathbf{h}(t)$ and relaxation terms to be zero. As expected, the corresponding eigenfrequencies coincide with the frequencies of coupled electron-nuclear spin waves, see Eq. (6), taken at $k = 0$. The electron and nuclear ac susceptibilities can be obtained from the same linearized equations by including the homogeneous rf magnetic field $\mathbf{h}(t)$.[56]

It what follows, we are interested in finding solutions of Eqs. (11-19) for arbitrarily large deviations of vectors $\mathbf{m}_{1,2}$ from their equilibrium orientations due to rf magnetic field at frequencies close to the q-NMR resonance. Following the previous work,[53] it is convenient to introduce a separate reference frame $x_1y_1y_1$ ($x_2y_2z_2$) for sublattice $\mathbf{M_1}$ ($\mathbf{M_2}$) obtained from the original frame xyz by a clockwise rotation around z-axis by angle ψ (by angle $\pi-\psi$), see Fig. 3, and chose new variables according to

$$\begin{aligned}
2M^{\xi} &= M_1^{x_1} + M_2^{x_2}, \quad 2m^{\xi} = m_1^{x_1} + m_2^{x_2},\\
2M^{\eta} &= M_1^{y_1} + M_2^{y_2}, \quad 2m^{\eta} = m_1^{y_1} + m_2^{y_2},\\
2M^{\zeta} &= M_1^{z_1} + M_2^{z_2}, \quad 2m^{\zeta} = m_1^{z_1} + m_2^{z_2},
\end{aligned} \tag{22}$$

where $M_i^{x_i}, M_i^{y_i}, M_i^{z_i}$ ($m_i^{x_i}, m_i^{y_i}, m_i^{z_i}$), $i = 1,2$, are components of electron (nuclear) magnetization vectors in the corresponding frame. The solutions of Eqs. (11-12) in these new variables can by found by linearizing Eqs. (11) with respect to transverse components of electron magnetization vectors, whose deviation from the equilibrium orientation is assumed to be small. This assumption is valid for sufficiently large magnetic fields $H > H_c$ where the oscillation of electron spins is only weakly affected by the hyperfine interaction with nuclei, see discussion in the previous section. The details of derivation are given in the Appendix. Finally, is is convenient to write the result in the coordinate system XYZ where the components of the net nuclear magnetization m_X, m_Y and m_Z are related to m^{ξ}, m^{η} and m^{ζ} by

$$\begin{aligned}
m^{\xi} &= m_X\cos\omega t + m_Y\sin\omega t,\\
m^{\eta} &= -m_X\sin\omega t + m_Y\cos\omega t,\\
M^{\zeta} &= m_Z,
\end{aligned} \tag{23}$$

which is somewhat similar to the usual rotating wave transformation used to describe traditional NMR.[57]

By omitting the relaxation terms in Eqs. (11-12) the equations for the net nuclear magnetization become (see Appendix for details)

$$\frac{\mathrm{d}m_X}{\mathrm{d}t} = \left(\omega_n - \omega - \omega_p\frac{m_Z}{m_0}\right) m_Y, \tag{24}$$

$$\frac{\mathrm{d}m_Y}{\mathrm{d}t} = -\left(\omega_n - \omega - \omega_p\frac{m_Z}{m_0}\right) m_X + \omega_1 m_Z, \tag{25}$$

$$\frac{\mathrm{d}m_Z}{\mathrm{d}t} = -\omega_1 m_Y, \tag{26}$$

where ω_1 is proportional to the amplitude of the rf magnetic field $\mathbf{h_1}$ and ω_p is the parameter discussed previously (see Eqs. (A14-15) in the Appendix for the precise definition of ω_1 and ω_p). Since the relaxation terms were neglected, the above equations can be used for description of the dynamics of the magnetization vector $\mathbf{m}$ only on the time intervals t which are small compared to the nuclear magnetic relaxation time. Note that, as was discussed previously from the microscopic point of view, the presence of the frequency pooling term $\omega_p(m_Z/m_0)$ does not allow us tp obtain large deflection angles of $\mathbf{m}$ from the equilibrium orientation by using a short rf pulse, as typically can be done in conventional NMR (the Rabi flopping).[57] Indeed, for typical experimental conditions we have $\omega_p >> \omega_1$, therefore the orientation of the axis of rotation of vector $\mathbf{m}$ in the frame XYZ changes quickly to be

nearly parallel to **Z** after applying the rf pulse. However, as we show below it is possible to obtain large angles of deflection by CW NMR. The description of the stationary state of the spin system under CW rf pumping requires to take into account the proper form of relaxation terms in Eqs. (11-12).

As discussed previously, the interaction between transverse components of the electron and nuclear magnetization vectors significantly changes the frequency of the nuclear spin oscillations. Another consequence of this interaction is the appearance of the relaxation of the transverse component of vector **m**. The indirect relaxation of this type has been studied previously but for relatively small amplitudes of **m**-vector oscillations when the nonlinear phenomena did not play any significant role.[49] Here, we consider the nonlinear equations of motion for the nuclear magnetization taking into account its indirect relaxation via the electron spin system.

Typically, the relaxation of the transverse component of magnetization occurs due to fluctuating magnetic fields acting on different spins and inhomogeneity of the external static magnetic field acting in the electron system. In what follows, we use an assumption that, because the nuclear spins experience an enormously large hyperfine field $H_e \sim 10^5$-10^6 Oe, we can neglect any other fields including fluctuating magnetic fields responsible for the relaxation of vectors $\mathbf{M_{1,2}}$. We can note immediately that the approximation $\mathbf{R}_{\mathrm{m_{1,2}}}$=0 in Eqs. (12) conserves the magnitude of the vectors $\mathbf{m_{1,2}}$, and therefore the net magnetization vector **m**. Thus, this approximation excludes the possibility of the heating of nuclear spin system under any processes including its excitation by rf pumping.

Using this approximation together with the assumption of small deviations of electron magnetization vectors from their equilibrium orientations at $H > H_c$, the equations of motion for the vector **m** become (see Appendix for details)

$$\frac{\mathrm{d}m_X}{\mathrm{d}t} = \left(\omega_n - \omega - \omega_p \frac{m_Z}{m_0}\right) m_Y - \frac{m_Z}{m_0}\frac{m_X}{T_{2n}}, \tag{27}$$

$$\frac{\mathrm{d}m_Y}{\mathrm{d}t} = -\left(\omega_n - \omega - \omega_p \frac{m_Z}{m_0}\right) m_X + \omega_1 m_Z - \frac{m_Z}{m_0}\frac{m_Y}{T_{2n}}, \tag{28}$$

$$\frac{\mathrm{d}m_Z}{\mathrm{d}t} = -\omega_1 m_Y - \frac{m_Z + m_0}{m_0}\frac{m_Z - m_0}{T_{2n}}, \tag{29}$$

where the nuclear transverse relaxation time T_{2n} is related to the electron transverse relaxation time T_2e by Eq. (A.13) in the Appendix.

The CW NMR signals are described by the stationary state solutions of the above equations. The latter are given by

$$\frac{m_X}{m_0} = \frac{(\omega_n - \omega - \omega_p + \omega_p\Delta)\,\omega_1\,(1-\Delta)}{(\omega_n - \omega - \omega_p + \omega_p\Delta)^2 + \Gamma_1^2}, \tag{30}$$

$$\frac{m_Y}{m_0} = \frac{\omega_1\Gamma_1\,(1-\Delta)}{(\omega_n - \omega - \omega_p + \omega_p\Delta)^2 + \Gamma_1^2}, \tag{31}$$

where $\Delta = 1 - m_Z/m_0$, which determines the longitudinal component of **m**, is the root of the fourth degree polynomial equation

$$\Delta(2-\Delta) = \frac{\omega_1^2\,(1-\Delta)^2}{(\omega_n - \omega - \omega_p + \omega_p\Delta)^2 + \Gamma_1^2}, \tag{32}$$

and Γ_1 is given by

$$\Gamma_1 = (1-\Delta)/T_{2n}. \tag{33}$$

For the sake of qualitative comparison with our theory, let us also consider the traditional Bloch approach in which the nuclear relaxation is described by introducing two phenomenological relaxation times, i.e. the longitudinal magnetization relaxation time T_1 and transverse magnetization relaxation time T_2.[57] Adding the corresponding relaxation terms into Eqs. (12), we obtain the phenomenological Bloch equations

$$\frac{\mathrm{d}m_X}{\mathrm{d}t} = \left(\omega_n - \omega - \omega_p \frac{m_Z}{m_0}\right) m_Y - \frac{m_X}{T_2}, \tag{34}$$

$$\frac{\mathrm{d}m_Y}{\mathrm{d}t} = -\left(\omega_n - \omega - \omega_p \frac{m_Z}{m_0}\right) m_X + \omega_1 m_Z - \frac{m_Y}{T_2}, \tag{35}$$

$$\frac{\mathrm{d}m_Z}{\mathrm{d}t} = -\omega_1 m_Y - \frac{(m_Z - m_0)}{T_1}. \tag{36}$$

Note that the above equations are obtained by disregarding the electron spin relaxation terms $\mathbf{R}_{\mathrm{M_{1,2}}}$ in Eqs. (11). The stationary state solutions of (34-36) can be written as

$$\frac{m_X}{m_0} = \frac{(\omega_n - \omega - \omega_p + \omega_p\Delta)\,\omega_1(1-\Delta)}{(\omega_n - \omega - \omega_p + \omega_p\Delta)^2 + T_2^{-2}}, \tag{37}$$

$$\frac{m_Y}{m_0} = \frac{\omega_1 T_2^{-1}(1-\Delta)}{(\omega_n - \omega - \omega_p + \omega_p\Delta)^2 + T_2^{-2}}, \tag{38}$$

where $\Delta = 1 - m_Z/m_0$, as defined earlier, is given by the roots of the third degree polynomial equation

$$\Delta = \frac{\omega_1^2 T_1 T_2^{-1}(1-\Delta)}{(\omega_n - \omega - \omega_p + \omega_p\Delta)^2 + T_2^{-2}}. \tag{39}$$

To distinguish between the two approximations which lead, on the one hand, to Eqs. (30-32), and, on the other hand, to Eqs. (37-39), we need to compare the continuous NMR signals predicted by these equations with the experimentally observed ones. This is done in the next section.

III. COMPARISON WITH EXPERIMENT

A. Experimental methods

In the experiment, we studied CW NMR signals in an easy-plane antiferromagnetic $MnCO_3$ sample at temperatures below 1 K. The sample was in the form of a rhombus-shaped plate about 0.7 mm thick, with diagonals of approximately 2.4 and 2.7 mm. The magnetic anisotropy axis **c** was perpendicular to the plane of the plate. The measured mass of the sample was about 8×10^{-3} g.

To excite continuous NMR signals in $MnCO_3$ by external rf pumping, the sample was placed in a high-quality factor rf resonator of a split-ring type.[58] The resonator and sample were oriented such that the external static magnetic field **H** and the rf magnetic field **h** of the resonator were perpendicular to each other and to the anisotropy axis **c** of the sample. The resonator was made of high-conductivity oxygen-free copper and had a resonant frequency of about 591.3 MHz and a quality factor of about 600 measured at 1 K. The input rf signal transmitted through a cryogenic low-loss semi-rigid coaxial cable was coupled to the resonator via a loop made at the end of the cable, and reflected signal was measured at different values of static field H and input rf power P using a network analyzer. The signals proportional to the in-phase and quadrature (with respect to the rf field in the cavity) components of ac magnetization induced in the sample could be extracted from the reflected signal. In order to avoid complications associated with the strong coupling of the spin system to the electro-magnetic mode of the resonator, which in particular leads to the normal mode splitting in the resonator reflection spectrum,[59] we used the frequency of rf pumping of 593.5 MHz, that is significantly detuned from the resonant frequency of the resonator. In this so called dispersive regime of coupling, the in phase (M_d) and quadrature (M_a) components of the ac magnetization are related to the complex amplitude (phasor) of the reflected signal according to

$$V \approx V_0 + C(-M_a + iM_d), \tag{40}$$

where V_0 is the complex amplitude of the signal reflected from an empty cavity, i is imaginary unit, and $C>0$ is a proportionality coefficient that depends on characteristics or resonator and its coupling to the rf transmission line.

B. Experimental results

Figure 4 shows the NMR signals proportional to M_a (absorption signal) and M_d (dispersion signal) measured at $T=735$ mK as a function of static field H at low input rf power of -50 dBm. At such a low power, the deviation of nuclear magnetization from its equilibrium orientation is very small. Correspondingly, the frequency pooling is very close to its value for the equilibrium spin system, therefore nonlinearity of the NMR signal is negligible. These signals are used to find the fitting parameters which define the dependence of the frequency pulling and nuclear magnetic relaxation rate on the value of H. It should be noted that although these signals were measured in the linear regime of NMR they are not ideally symmetric. This suggests that the sample used in the experiment is not a single crystal, which is also confirmed by its careful visual examination under the microscope. It is likely that the sample consists of at least two or three mono-crystals of different size with somewhat different orientations of their lattices with respect to each other.

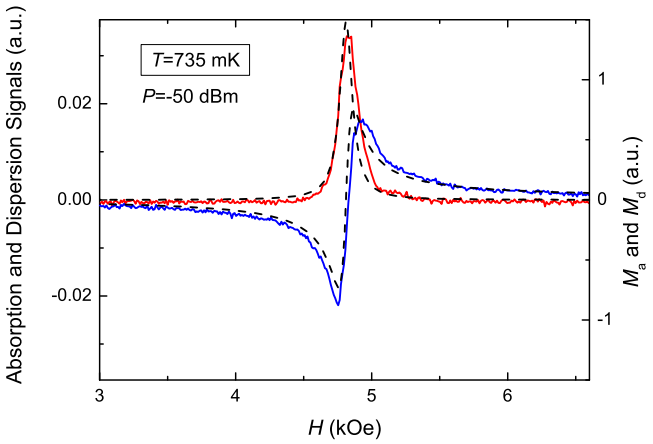

FIG. 4: (color online) Absorption (solid line, red) and dispersion (solid line, blue) signals measured in $MnCO_3$ at $T=735$ mK and at low input rf power of $P=-50$ dBm. Dashed lines are the ac magnetization components M_a and M_d calculated as described in Section III(C).

Figures 5 and 6 show the absorption and dispersion signals measured at $T=735$ mK and at different input rf power levels. It is clear that with increasing power the NMR frequency shifts towards lower values of H due to the frequency pulling. Both the absorption and dispersion signals attain very asymmetrical shape. In addition, both signals show strong hysteresis upon reversing the direction of the field sweep. In Figure 7 we show the absorption and dispersion signals obtained at the highest input power of $P=0$ dBm used in this experiment. In the next section we show comparison of the measured absorption an dispersion signals with predictions of our theory, see Eqs. (30-32). In addition, we compare the experimental results with predictions based on the phenomenological Bloch equations, see Eqs. (37-39).

C. Expressions for ac magnetization components and their comparison with experimental results

In order to compare the results presented in Figs. (5-6) with predictions of our theory, first we need to find relation between the ac magnetization components M_a and M_d and components of nuclear magnetization m_X and m_Y described by Eqs. (30-31). It is important to realize that due to the much larger magnitude of the electron magnetization vector $\mathbf{M}=(M^\xi, M^\eta, M^\zeta)$ compared to that of the nuclear magnetization vector $\mathbf{m}=(m^\xi, m^\eta, m^\zeta)$, whose ratio is approximately

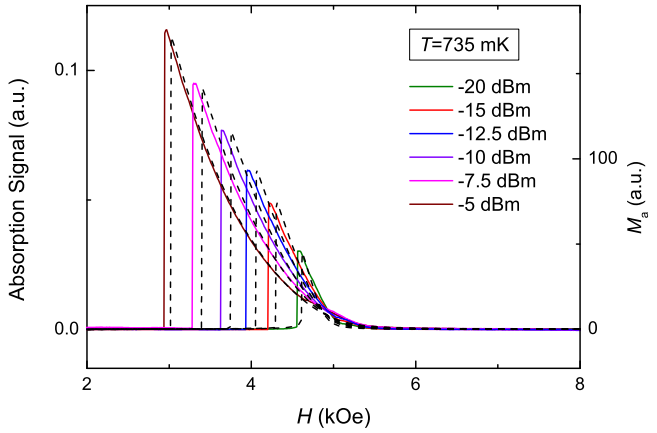

FIG. 5: (color online) Absorption signals (solid lines) measured in $MnCO_3$ at $T = 735$ mK and at several values of input rf power (shown in the figure) during down-field sweep. Dashed lines represent values of M_a calculated as described in Section III(C).

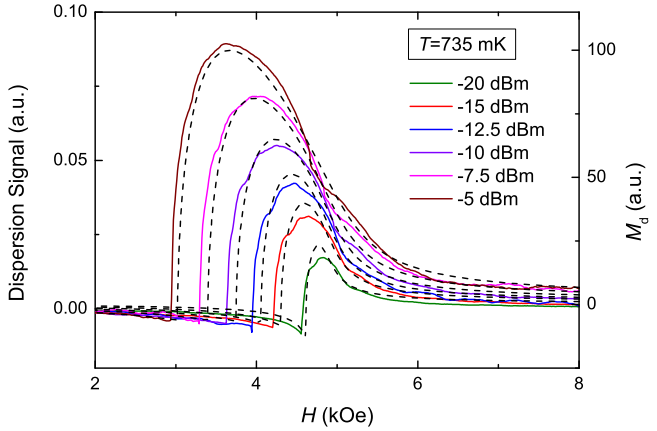

FIG. 6: (color online) Dispersion signals measured in $MnCO_3$ at $T = 735$ mK and at several values of input rf power (shown in the figure) during down-field sweep. Dashed lines represent values of M_d calculated as described in Section III(C).

$\gamma_e/\gamma_n \gtrsim 10^3$, the main contribution to the observed ac magnetization comes from the oscillations of vector $\mathbf{M}$. We can find needed relations using relation between the complex amplitudes of $M^{\xi}(t)$ and $m^{\xi}(t)$, as given by Eq. (A.7-A.9) in the Appendix.

According to Fig. 3 and Eqs. (20-22), the vector component of electron magnetization $\mathbf{M}_{\parallel}(t) \parallel \mathbf{h}(t)$, which defines the observed NMR signals, can be expressed in terms of $M^{\xi}(t)$ as

$$M(t) = M_1^z + M_2^2 = -(M_1^{x_1} + M_2^{x_2}) \sin\psi = \\ = -2\left(\frac{H + H_D}{H_E}\right) M^{\xi}(t). \qquad (41)$$

Assuming the time dependence of the rf magnetic field in the form $h(t) = 2H_1 \cos\omega t$, the absorption M_a and dispersion M_d signals are given by, respectively, the imaginary and real parts of the complex amplitude of $M_{\parallel}(t)$. The expressions for M_d

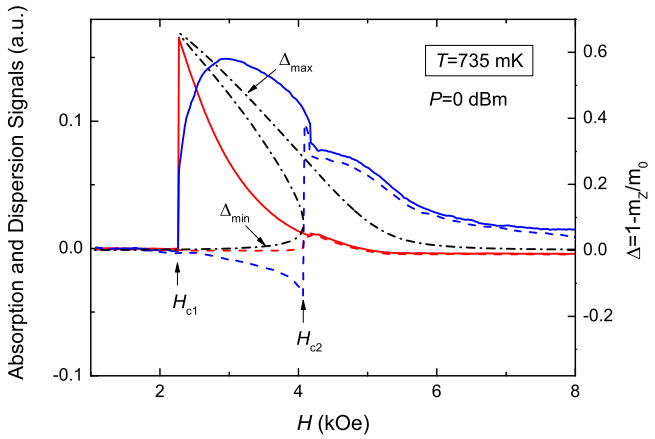

FIG. 7: (color online) Absorption and dispersion signals measured at $T = 735$ mK at highest input rf power of $P = 0$ dBm during up-field (dashed lines) and down-field (solid lines) sweeps. The dash-dotted line is the result of numerical calculations for $\Delta = 1 - m_Z/m_0$ as described in Section III(C).

and M_a in terms of oscillating components of the nuclear magnetization vector can be found from the above equation using Eqs. (A.7-A.9) in the Appendix. Using the transformation (23) and expressing results in terms of nuclear magnetization vector components m_X and m_Y we obtain

$$M_d = M_d^{nr} + \frac{H_n}{H}\left(1 - \frac{\omega^2}{\omega_e^2}\right)^{-1}\left[m_X - \frac{\omega}{\omega_n \omega_p T_{2n}} m_Y\right], \\ M_a = \frac{H_n}{H}\left(1 - \frac{\omega^2}{\omega_e^2}\right)^{-1}\left[m_Y + \frac{\omega}{\omega_n \omega_p T_{2n}} m_X\right]. \qquad (42)$$

In the above equations, the non-resonant contribution M_d^{nr} to the dispersion signal is given by

$$M_d^{nr} = \frac{H_1 H_n}{H^2}\left(1 - \frac{\omega^2}{\omega_e^2}\right)^{-2} \frac{\omega_n}{\omega_p} m_0. \qquad (43)$$

It arises from the direct coupling of the electron magnetization vector to the rf magnetic field having amplitude H_1. The resonant (at the NMR frequency) contribution comes from the terms containing m_X and m_Y. The main contribution to the dispersion (absorption) signal comes from the m_X (m_Y) component of the nuclear magnetization vector. Note that it is enhanced by the amplification factor η given by Eq. (A.11) in the Appendix. The components m_X and m_Y are given by equations (30-31) and are expressed in terms of the dimensionless parameter $\Delta = 1 - m_Z/m_0$ determined from Eq. (32). It is instructive to discuss the general form of the solutions of this equations. Eq. (32) is a fourth order polynomial equation with respect to Δ. One of the roots of Eq. (32), viz. $\Delta \approx 2$, corresponds to unstable state with antiparallel orientation of the vectors $\mathbf{m}$ and $\mathbf{H_n}$. The other three roots are the solutions of a third order polynomial equation which is obtained from (32) by excluding the root $\Delta \approx 2$. We are interested in the real-valued roots and their dependence on H, which is defined by

the corresponding dependencies of $\omega_1(H)$, $\omega_p(H)$ and $T_{2n}(H)$ given by Eqs. (A.10-A.13) in the Appendix.

At low rf excitation powers such that $\omega_1 T_{2n} \ll 1$ the equation (32) has only one real root given by

$$\Delta_1 = \frac{\omega_1^2}{(\omega_n - \omega - \omega_p)^2 + T_{2n}^{-2}} \ll 1. \quad (44)$$

Using this expression in Eqs. (30-31) we obtain

$$\frac{m_X}{m_0} = \frac{(\omega_n - \omega - \omega_p)\omega_1}{(\omega_n - \omega - \omega_p)^2 + T_{2n}^{-2}},$$
$$\frac{m_Y}{m_0} = \frac{\omega_1 T_{2n}^{-1}}{(\omega_n - \omega - \omega_p)^2 + T_{2n}^{-2}}. \quad (45)$$

At fixed rf frequency ω the position of the resonance in static magnetic field H is determined by the dependence of ω_p on H given by Eq. (A.12) in the Appendix. The resonance value of field $H = H_{res}$ is defined by

$$\omega_n - \omega - \omega_p(H_{res}) = 0. \quad (46)$$

The width of the resonance ΔH, which can be defined as the distance between the maximum and minimum of the dispersion signal, is related to T_{2n} as

$$T_{2n}^{-1}(H_{res}) = -\frac{1}{2}\frac{\partial \omega_p(H_{res})}{\partial H}\Delta H. \quad (47)$$

The dependence of T_{2n} on H is given by Eq. (A.13) in the Appendix. It is convenient to express the dependence of ω_p and T_{2n} on H in terms of adjustable parameters a_1 and a_2 as

$$\omega_p(H) = \frac{a_1}{H(H+H_D)}, \quad (48)$$
$$T_{2n}^{-1}(H) = \frac{a_2}{H^2(H+H_D)^2}, \quad (49)$$

and determine the numerical values of a_1 and a_2 at given temperature from the comparison of experimental data taken at low rf excitation power and the ac magnetization components M_a and M_d calculated using Eqs. (42) and (45). Such comparison is shown in Fig. 4 where the M_a and M_d calculated using $a_1/2\pi = 2.06\times10^3\,\mathrm{MHz(kOe)^2}$ and $a_2/2\pi = 1.6\times10^3\,\mathrm{MHz(kOe)^4}$ are plotted by the dashed lines. Here, we used $H_D = 4.4\,\mathrm{kOe}$, $\omega_n/2\pi = 640\,\mathrm{MHz}$, and $\omega/2\pi = 593.5\,\mathrm{MHz}$. The value of H_1 was chosen to be sufficiently small to ensure a linear NMR regime. The corresponding values of H_{res} and ΔH are approximately 4.81 kOe and 0.11 kOe, respectively. The width of the resonance corresponds to the nuclear relaxation T_{2n} time of approximately $0.19\,\mu\mathrm{s}$.

For arbitrarily large rf excitation powers there exists a range of H where there are more than one real-valued roots of Eq. (32). The numerical solution of this equation for a large value of H_1 is shown by the dash-dotted line in Fig. 7. In this calculation, we used $\omega_p(H)$ and $T_{2n}(H)$ given by Eqs. (48-49) with numerical values of a_1 and a_2 given above. The interval $H_{c1} < H < H_{c2}$ corresponds to the region where three real roots exist. The merging point of two real roots (where they become complex) corresponds to the phenomenon which in mathematics is called *catastrophe*. We restrict ourselves to the analysis of the upper branch $\Delta_{max}(H)$ which has the critical point at $H = H_{c1}$, see Fig. 7. The state of the lower branch $\Delta_{min}(H)$ is destroyed at the fields $H < H_{c2}$ due to instabilities caused by the excitation of n-magnons which are in resonance with the rf pumping field.[60,61]

In order to make comparison between the experimental data presented in Figs. 5-6 and the ac magnetization components M_a and M_d calculated using Eqs. (30-32,42) we need to establish correspondence between, on the one hand, the values of rf excitation power used in the experiment and, on the other hand, the numerical values of H_1 used in the calculations. We used the value of $H_{c_1} \approx 2.2\,\mathrm{kOe}$ in Fig. 7 to define the value of $H_1 = 23\,\mathrm{Oe}$ at the excitation power of 0 dBm. The lineshapes of M_a and M_d calculated for the corresponding values of H_1 and using Eqs. (48) and (49) are plotted in Figs. 5 and 6, respectively, by the dashed lines. As seen in these figures, we obtain a very good quantitative agreement between our experimental data and predictions of our theoretical model based on Eqs. (27-29). Note that the conservation of the magnitude of vector **m**, which follows from our theory, allows us to express $\Delta_{max}(H)$ in terms of the deflection angle β between the vector **m** and its equilibrium orientation

$$\Delta_{max}(H) = 1 - \cos\beta. \quad (50)$$

At the critical field $H_{c1} \approx 2.2\,\mathrm{kOe}$ in Fig. 7 corresponding to the input rf power of 0 dBm the deflection angel has value $\beta \approx 70$ degrees.

For the sake of comparison with the predictions of the Bloch model based on equations (34-36) it is instructive to consider dependence of the absorption signal M_a at $H = H_{c1}$ on the input rf power P. Note that the critical field $H = H_{c_1}$ corresponds to the resonant condition

$$\omega_n - \omega - \omega_p + \omega_p\Delta = 0. \quad (51)$$

From Eqs. (30-31) for the steady state solutions this gives $m_X(H_{c_1}) = 0$ and $m_Y(H_{c_1}) = m_0\omega_1 T_{2n}$, therefore from the second line of (42) and Eqs. (A.10-A.13) in the Appendix we obtain

$$M_a(H_{c_1}) = \frac{\gamma_n m_0 H_n^2}{a_2}\left(1 - \frac{\omega^2}{\omega_e^2}\right)^{-2}(H_{c_1} + H_D)^2 H_1. \quad (52)$$

In order to get rid of the field-independent factor in front of the right-hand side of the above equation, it is convenient to normalize this expression to the value of $M_a(H_{c1})$ at one of the values of the input rf power used in the experiment. For example, we choose the lowest power of $P^* = -20\,\mathrm{dBm}$ used

in Fig. 5. The expression for the normalized absorption signal becomes (for the sake of simplicity we neglect $\omega/\omega_e << 1$)

$$\frac{M_a(H_{c1})}{M_a^*(H_{c1})} \approx \left(\frac{H_{c1}+H_D}{H_{c1}^*+H_D}\right)^2 \frac{H_1}{H_1^*} = \alpha(H_{c_1}, \sqrt{P/P^*}), \quad (53)$$

where M_a^*, H_{c1}^* and H_1^* are the corresponding values of M_a, H_{c1} and H_1 at the input rf power $P = P^*$. Note that the normalized absorption signal depends only on the values of the critical field H_{c1} and the ratio $\sqrt{P/P^*} = H_1/H_1^*$, which can be readily determined in the experiment. Figure 8 shows dependence of $M_a(H_{c1})/M_a^*(H_{c1})$ on $\alpha(H_{c1}, \sqrt{P/P^*})$ obtained from the experimental data shown in Figs. 5 and 7 (opened squares), as well as theoretically predicted dependence given by Eq. (53) (dashed line).

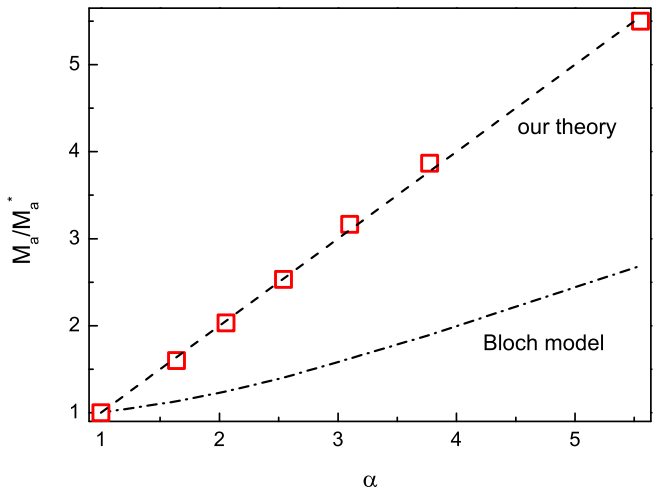

FIG. 8: (color online) Normalized values of the absorption signal at the critical field $H = H_{c1}$ as a function of quantity $\alpha(H_{c1}, \sqrt{P/P^*})$ defined by Eq. (53) obtained from the experimental data presented in Figs. 5 and 7 (opened squares). The lines are the corresponding dependences predicted by our theory (dashed line) and by the conventional Bloch approach (dash-dotted line).

Now we compare this result with predictions of the heating scenario based on the phenomenological Bloch equations (34-36). Note that similar to Eq. (32), the third order polynomial equation (39) with respect to Δ can have three real-valued roots in certain ranges of the static magnetic field $H_{c1} < H < H_{c2}$. This may result in the nonlinear NMR signals similar to those described earlier.[16] Using condition (51) satisfied at the field $H = H_{c1}$, we obtain from Eqs. (37-39)

$$m_x(H_{c1}) = 0, \quad m_y(H_{c1}) = \omega_1 T_2 m_z(H_{c1}),$$
$$m_Z(H_{c1}) = \frac{m_0}{1+\omega_1^2 T_1 T_2}. \quad (54)$$

Note that, unlike in our proposed theory, the Bloch model does not conserve the magnitude of magnetization vector. Indeed, from Eq. (54) we have

$$|\mathbf{m}| = \sqrt{\frac{1+\omega_1^2 T_2^2}{\left(1+\omega_1^2 T_1 T_2\right)^2}} m_0. \quad (55)$$

Typically, we have $T_2 \ll T_1$, therefore $|\mathbf{m}|$ can be significantly less than m_0 already for $\omega_1^2 T_1 T_2 \gtrsim 1$.

Using Eqs. (51,54) it is convenient to write $\omega_1^2 T_1 T_2$ as

$$\omega_1^2 T_1 T_2 = \frac{\Delta\omega(H_{c1})}{\omega_p(H_{c1}) - \Delta\omega(H_{c1})}, \quad (56)$$

where $\Delta\omega = \omega - \omega_n + \omega_p$. Note that using the above equation, the values of $\omega_1^2 T_1 T_2$ at $H = H_{c1}$ can be determined from the experimental values of H_{c_1}. Using the second line of Eq. (42) we obtain expression for the absorption signal at the catastrophe field

$$M_a(H_{c_1}) = \frac{m_0 H_n}{H}\sqrt{\frac{T_2}{T_1}}\left(1-\frac{\omega^2}{\omega_e^2}\right)^{-1}\frac{\sqrt{\omega_1^2 T_1 T_2}}{1+\omega_1^2 T_1 T_2}, \quad (57)$$

and using Eqs. (A.10-A.11) from the Appendix and definition of α, see Eq. (53), we obtain for the normalized absorption signal

$$\frac{M_a(H_{c1})}{M_a^*(H_{c1})} \approx \left(\frac{H_{c1}^*(H_{c1}^*+H_D)}{H_{c1}(H_{c1}+H_D)}\right)^2 \frac{1+(\omega_1^2 T_1 T_2)^*}{1+\omega_1^2 T_1 T_2}\alpha, \quad (58)$$

where $\left(\omega_1^2 T_1 T_2\right)^*$ is the value of $\omega_1^2 T_1 T_2$ at the critical field for the input rf power $P = P^*$. Again, note that the term in front of α on the right-hand side of the above equation depends only on the value of the critical field $H = H_{c1}$, which can be determined from the experiment, and does not depend on the choice of the values for T_1 and T_2. The dependence of the normalized absorption signal on α given by Eq. (58) is plotted in Fig. 8 by a dash-dotted line. Clearly, the conventional Bloch approach fails to adequately account for the behavior observed in the experiment. Using Eq. (56), it is straightforward to estimate the value of $\omega_1^2 T_1 T_2$ at the critical field $H = H_{c1}$ for the maximum input rf power $P = 0\,\mathrm{dBm}$. Using the value of $H_{c1} \approx 2.2\,\mathrm{kOe}$, see Fig. 7, we obtain $\omega_1^2 T_1 T_2 \approx 2$. Thus, the Bloch theory predicts significant reduction of the magnitude of the nuclear magnetization vector due to the heating. This does not agree with our experimental results.

IV. CONCLUSIONS

We suggest the description of the coupled electron-nuclear spin systems by the coupled Landau-Lifshitz-Gilbert equations which take into account an indirect relaxation of nuclear spins via the electron spin subsystem. In our theory the magnitude of the nuclear magnetization is conserved for arbitrary large excitation powers, which is drastically different from the

conventional heating scenario based on the phenomenological Bloch approach. In particular, we consider the coupled electron-nuclear spin motion in the easy-plane antiferromagnetic crystals with a weak magnetic anisotropy in the basal plain. The equations of motion are solved analytically assuming small deviations of the electron magnetization vectors from their equilibrium orientations, which allows us to linearize the corresponding equations of motion for the electron subsystem. The obtained solutions are compared with the experimental nonlinear NMR signals obtained in a $MnCO_3$ sample at temperatures below 1 K and good quantitative agreement is found. This suggests that at high excitation rf powers used in the experiment the nuclear magnetization vector can be deflected by very large angles exceeding 70 degrees. This result is drastically different from predications of the standard heating scenario based on the phenomenological Bloch approach. In particular, the latter predicts significant reduction of the magnitude of the nuclear magnetization vector under conditions of our experiment. The proposed theory brings together the properties of nonlinear NMR in, on the one hand, the magnetic systems in solids considered here and, on the other hand, the superfluid ^{3}He where the magnitude of the nuclear magnetization vector is also conserved. This provides the theoretical background for the mechanism of formation of a BEC of non-equilibrium magnons in $MnCO_3$. This topic is currently under the theoretical and experimental investigation.

Acknowledgements The work of L. V. A and D. K. was supported by an internal grant from the Okinawa Institute of Science and Technology Graduate University and JSPS KAKENHI (Grant No. 26400340). The work of Yu. M. B. and R. R. G. was supported by the Russian Science Foundation (Grant RSF 16-12-10359). Part of the work is done by the order of FASO of the RF: subject "Spin" No 01201463332, grant No 15-9-2-49; subject "Electron No 01201463326, grant No 15-8-2-10. Yu. M. B acknowledges support from the Okinawa Institute of Science and Technology Graduate University as a visiting scientist. We thank Jason Ball for proofreading the manuscript.

Appendix: Equations for coupled electron-nuclear spin oscillations

The system of coupled equations (11-12) contains twelve dynamical variables corresponding to three components for each of four magnetization vectors $\mathbf{M}_{1,2}$ and $\mathbf{m}_{1,2}$. This system conveniently splits into two independent subsystems, each consisting of six equations, if we introduce new dynamical variables according to[53]

$$2M^{\alpha_\pm} = M_1^{\alpha_1} \pm M_2^{\alpha_2}, \quad 2m^{\alpha_\pm} = m_1^{\alpha_1} \pm m_2^{\alpha_2}, \tag{A.1}$$

where the upper indexes are defined as $\alpha_\pm \in [x_\pm, y_\pm, z_\pm]$, $\alpha_1 \in [x_1, y_1, z_1]$, $\alpha_2 \in [x_2, y_2, z_2]$, and $M_i^{x_i}$, $M_i^{y_i}$, $M_i^{z_i}$ ($m_i^{x_i}$, $m_i^{y_i}$, $m_i^{z_i}$), $i = 1, 2$, are components of electron (nuclear) magnetization vectors in the corresponding reference frames (x_1, y_1, z_1) and (x_2, y_2, z_2) defined in Fig. 3. The components M^{α_-} correspond to the high-frequency branch of oscillations of the vectors $\mathbf{M}_{1,2}$, which is weakly affected by the interaction between electron and nuclear spins. For this reason, only the low-frequency branch of $\mathbf{M}_{1,2}$ is of interest for NMR. This branch is described by the components M^{α_+} and m^{α_+}. It is convenient to mark the indexes x_+, y_+ and z_+ as, respectively, ξ, η and ζ. In what follows, we consider the static magnetic fields $H > H_c$ at which the deflection angles of the vectors $\mathbf{M}_{1,2}$ from their equilibrium orientation are small, see discussion in Section II, which corresponds to the following approximation for the components of vector $\mathbf{M}$

$$M^{\xi,\eta} \ll M_0, \quad M^{\zeta} \approx M_0, \tag{A.2}$$

where M_0 is the magnitude of vectors $\mathbf{M}_1$ and $\mathbf{M}_2$. In this approximation, the linearized equations of motion for M^ξ and M^η become[53]

$$\begin{aligned}
&\frac{1}{\gamma_e}\frac{\mathrm{d}M^\xi}{\mathrm{d}t} = (H_E + H_A)M^\eta - H_n m^\eta - \frac{1}{\gamma_e T_{2e}}M^\xi, \\
&\frac{1}{\gamma_e}\frac{\mathrm{d}M^\eta}{\mathrm{d}t} = -\frac{H(H+H_D)}{H_E}M^\xi + \\
&+\frac{H+H_D}{H_E}M_0 h(t) + H_n m^\xi - \frac{1}{\gamma_e T_{2e}}M^\eta,
\end{aligned} \tag{A.3}$$

where T_{2e} is the transverse relaxation time of the electron magnetization. We will use the applied rf magnetic field $\mathbf{h} \parallel \mathbf{z}$ in the form

$$h(t) = 2H_1 \cos\omega t, \tag{A.4}$$

Note that the approximation (A.2) used to obtain linearized Eqs. (A.3) corresponds to the following condition

$$|\omega - \omega_e| T_{2e} \gg 1, \tag{A.5}$$

where $\omega_e = \gamma_e H(H + H_D)$ is the frequency of uniform precession of vector $\mathbf{M}$ neglecting the interaction between electron and nuclear spins. The condition (A.5) is well satisfied for typical rf frequencies close to the NMR frequency, and thus significantly lower than electron-spin resonance frequency.

The equations (A.3) can be simplified further. Noting that, since $M^\eta \gg m^\eta$ and $(H_E + H_A)T_{2e} \gg 1$, we can neglect the last two terms in the right-hand side of the first equation in (A.3). Moreover, since typically $H_E \sim 10^5$-10^7 Oe and $H_A \sim 10^2$-10^4 Oe, we can neglect H_A comparing with H_E. Using these approximations, we obtain from (A.3)

$$\begin{aligned}
&\frac{\mathrm{d}^2 M^\xi}{\mathrm{d}t^2} + \frac{2}{T_{2e}}\frac{\mathrm{d}M^\xi}{\mathrm{d}t} + \omega_e^2 M^\xi = \\
&= 2\gamma_e^2 (H + H_D) M_0 H_1 \cos(\omega t + \psi_0) + \gamma_e^2 H_n H_E m^\xi.
\end{aligned} \tag{A.6}$$

As usual, it is convenient to look for the solutions of the above equation in the complex form $M^\xi(t) = M_\omega^\xi e^{i\omega t}$ and

$m^{\xi}(t) = m^{\xi}_{\omega} e^{i\omega t}$, where M^{ξ}_{ω} and m^{ξ}_{ω} are the complex amplitudes (phasors) of oscillating components $M^{\xi}(t)$ and $m^{\xi}(t)$. Using the rotating wave approximation,[57] it is straightforward to obtain

$$M^{\xi}_{\omega} \approx M^{\xi}_{\omega}(H_1) + M^{\xi}_{\omega}(m^{\xi}_{\omega}), \tag{A.7}$$

$$M^{\xi}_{\omega}(H_1) = \frac{M_0}{\omega_n}\omega_1, \tag{A.8}$$

$$M^{\xi}_{\omega}(m^{\xi}_{\omega}) = \frac{2M_0}{\omega_n}\left(\omega_p - i\frac{\omega}{T_{2n}\omega_n}\right)\frac{m^{\xi}_{\omega}}{m_0}, \tag{A.9}$$

where for the sake of convenience we use the following definitions

$$\omega_1 = \gamma_n \eta H_1, \tag{A.10}$$

$$\eta = \frac{H_n}{H}\left(1 - \frac{\omega^2}{\omega_e^2}\right)^{-1}, \tag{A.11}$$

$$\omega_p = \frac{\omega_n}{2}\frac{H_n H_E}{H(H+H_D)}\frac{m_0}{M_0}\left(1 - \frac{\omega^2}{\omega_e^2}\right)^{-1}, \tag{A.12}$$

$$\frac{1}{T_{2n}} = \frac{2\omega_n\omega_p}{T_{2e}\omega_e^2}\left(1 - \frac{\omega^2}{\omega_e^2}\right)^{-1}. \tag{A.13}$$

To obtain the above equations, we used expansion in small parameter $\omega/T_{2e} \ll (\omega_e^2 - \omega^2)$. The influence of the relaxation is described by the imaginary part of M^{ξ}_{ω} in (A.9). Note that the above equations satisfy the condition $\mathrm{Im}(M^{\xi}_0) = 0$ which means the absence of dissipation at $\omega = 0$. It is important to fulfill this strict requirement imposed by the theory of irreversible processes.

The approximations used to obtain Eq. (A.6) allows us to write Eqs. (12) in terms of components (22) of the nuclear magnetization vector in the form

$$\frac{\mathrm{d}m^{\xi}}{\mathrm{d}t} = \omega_n m^{\eta}, \quad \frac{\mathrm{d}m^{\eta}}{\mathrm{d}t} = -\omega_n m^{\xi} + \omega_n \frac{M^{\xi}}{M_0} m^{\zeta},$$
$$\frac{\mathrm{d}m^{\zeta}}{\mathrm{d}t} = -\omega_n \frac{M^{\xi}}{M_0} m^{\eta}. \tag{A.14}$$

In the above equations, the harmonic dependence of the components $m^{\xi}(t)$, $m^{\eta}(t)$ and $m^{\zeta}(t)$ due to the rf magnetic field (A.4) comes from the terms containing $M^{\xi}(t)$. As usual, it is convenient to get rid of the harmonic time-dependent terms by applying the transformation given by Eq. (23). Note that in terms of transformed coordinates m_X, m_Y and m_Z the complex amplitude of $m^{\xi}(t)$ appearing in Eq. (A.9) can be written as $m^{\xi}_{\omega} = (m_X - i m_Y)/2$. Using this transformation and Eqs. (A.7-A.13), it is straightforward to obtain Eqs. (27-29) discussed in the main text.

* Current address: London Center for Nanotechnology, University College London, London WC1H 0AH, United Kingdom
† Electronic address: denis@oist.jp

[1] H. Suhl, Phys. Rev. **109**, 606 (1958); T. Nakamura, Prog. Theor. Phys. (Kyoto) **20**, 542, (1958).
[2] K. Lee, A. M. Portis, and G. L. Witt, Phys. Rev. **132**, 144 (1963); G. L. Witt and A. M. Portis, Phys. Rev. **135**, A1616 (1964).
[3] A. J. Heeger and D. T. Teaney, J. Appl. Phys. **35**, 846 (1964).
[4] D. Shaltiel, Phys. Rev. **142**, 300 (1966).
[5] V. Minkiewicz and A. Nakamura, Phys. Rev. **143**, 361 (1966).
[6] L. B. Welsh, Phys. Rev. **156**, 370 (1967).
[7] V. A. Tulin, Sov. Phys. JETP **28**, 431 (1969).
[8] A. J. Heeger, A. M. Portis, D. T. Teaney, and G. Witt, Phys. Rev. Lett. **7**, 307 (1961).
[9] D. Shalteil and H. J. Fink, J. Appl. Phys. **35**, 848 (1964).
[10] Kh. G. Bogdanova, V. A. Golenischev-Kutuzov, F. S. Vagapova, A. A. Monakhov, and R. V. Saburova, Sov. Phys. JETP **41**, 919 (1975).
[11] Yu.M.Bunkov, B.S.Dumesh, Sov. Phys. JETP **68** 1161 (1975).
[12] Yu.M.Bunkov, B.S.Dumesh, M.I.Kurkin, JETP Letters **19**, 132 (1974).
[13] Yu.M.Bunkov, V.V.Dmitriev, Sov Phys. JETP **53**, 1237 (1981).
[14] Yu.M.Bunkov, JETP Letters **23**, 244 (1976).
[15] P. M. Richards, C R. Christensen, B. D. Guenther, and A. C. Daniel, Phys. Rev. B **4**, 2216 (1971).
[16] P. G. de Gennes, P. A. Pinkus, F. Hartmann-Boutron, and J. M. Winter, Phys. Rev. **129**, 1105 (1963).
[17] A.S. Borovik-Romanov, Yu.M. Bunkov, B.S. Dumesh, M.I. Kurkin, M.P. Petrov, V.P. Chekmarev, Physics-Uspekhi **142**, 537 (1984).
[18] A.S. Borovik-Romanov, Yu.M. Bunkov, V.V. Dmitriev, Yu.M. Mukharskii, JETP Lett. **40**, 1033 (1984).
[19] I.A. Fomin, JETP Lett. **40**, 1037 (1984).
[20] Yu. M. Bunkov and G. E. Volovick, J. Low Temp. Phys. **150**, 135 (2008).
[21] S. O. Demokritov, V. E. Demidov, O. Dzyapko, G. A. Melkov, A. A. Serga, B. Hillebrands, and A. N. Slavin, Nature **443**, 430 (2006).
[22] D. A. Bozhko, A. A. Serga, P. Clausen, V. I. Vasyuchka, F. Heussner, G. A. Melkov, A. Pomyalov, V. S. L'vov, and B. Hillebrands, Nature Physics **12**, 1057 (2016).
[23] R.R.Gazizulin, Yu.M.Bunkov, V. L. Safonov, JETP Letters **102**,

876 (2015).
[24] E. A. Donley, N. R. Claussen, S. L. Cornish, J. L. Roberts, E. A. Cornell, and C. E. Wieman, Nature **412**, 295 (2001).
[25] Yu.M. Bunkov, G.E. Volovik, Europhys. Lett. **21**, 837 (1993).
[26] A.S. Borovik-Romanov, Yu.M. Bunkov, V.V. Dmitriev, Yu.M. Mukharskiy, D.A. Sergatskov, Phys. Rev. Lett. **62**, 1631 (1989).
[27] A.S. Borovik-Romanov, Yu.M. Bunkov, A. de Waard, V.V. Dmitriev, V. Makroczyova, Yu.M. Mukharskiy, D.A. Sergatskov, JETP Letters **47**, 478 (1988).
[28] A.S. Borovik-Romanov, Yu.M. Bunkov, V.V. Dmitriev, Yu.M. Mukharskiy, D.A. Sergatskov, Physica B **165**, 649 (1990).
[29] Yu.M. Bunkov, V.V. Dmitriev, Yu.M. Mukharskiy, JETP Letters **43**, 168 (1986).
[30] Yu.M. Bunkov, V.V. Dmitriev, Yu.M. Mukharskiy, Physica B **178**, 196 (1992).
[31] M. Kupka, P. Skyba, Phys. Rev. B **85**, 184529 (2012).
[32] Yu.M. Bunkov, "Spin Supercurrent and Novel Properties of NMR in ^{3}He" in Prog. Low Temp. Phys. **14**, ed. W.P. Halperin, Elsevier (1995).
[33] I.A. Fomin, "Pulsed NMR and the spatially nonuniform precession of spin in the superfluid phases of ^{3}He", in Helium Three **9**, eds. W.P. Halperin and L.P. Pitaevskii, Elsevier (1990).
[34] Yu.M. Bunkov, J. Low Temp. Phys. **135**, 337 (2004).
[35] Yu.M. Bunkov, J. Phys.: Cond. Matter **21**, 164201 (2009).
[36] Yu.M. Bunkov, G.E. Volovik, J. Phys.: Cond. Matter **22**, 164210 (2010).
[37] Yu.M. Bunkov, G.E. Volovik, "Spin superfluidity and magnon BEC", Chapter IV of the book "Novel Superfluids", eds. K.H. Bennemann and J.B. Ketterson, Oxford University Press (2013).
[38] I.A. Fomin, JETP Letters **39**, 466 (1984).
[39] A.S. Borovik-Romanov, Yu.M. Bunkov, V.V. Dmitriev, Yu.M. Mukharskiy, JETP Letters **39**, 469 (1984).
[40] Yu.M. Bunkov, V.V. Dmitriev, Yu.M. Mukharskiy, Sov. Phys. JETP **61**, 719 (1985).
[41] T. Kunimatsu, T. Sato, K. Izumina, A. Matsubara, Y. Sasaki, M. Kubota, O. Ishikawa, T. Mizusaki, Yu.M. Bunkov, JETP Letters **86**, 244 (2007).
[42] J. Elbs, Yu.M. Bunkov, E. Collin, H. Godfrin, G.E. Volovik, Phys. Rev. Lett. **100**, 215304 (2008).
[43] T. Sato, T. Kunimatsu, K. Izumina, A. Matsubara, M. Kubota, T. Mizusaki, Yu.M. Bunkov, Phys. Rev. Lett. **101**, 055301 (2008).
[44] P. Hunger, Yu.M. Bunkov, E. Collin, H. Godfrin, J. Low Temp. Phys. **158**, 129 (2010).
[45] Yu.M. Bunkov, Physics-Uspekhi **53**, 843 (2010).
[46] Yu.M. Bunkov, E.M. Alakshin, R.R. Gazizulin, A.V. Klochkov, V.V. Kuzmin, T.R. Safin, M.S. Tagirov, JETP Letters **94**, 68 (2011).
[47] Yu.M. Bunkov, E.M. Alakshin, R.R. Gazizulin, A.V. Klochkov, V.V. Kuzmin, V.S. L'vov, M.S. Tagirov, Phys. Rev. Lett. **108**, 177002 (2012).
[48] E. M. Alakshin, Yu. M. Bunkov, R. R. Gazizulin et al., Journal of Physics: Conference Series **568**, 042001 (2014).
[49] E.A. Turov, M.P. Petrov, *Nuclear Magnetic Resonance in Ferro- and Antiferromagnets* (Halsted Press, New York, 1972).
[50] M. Borich, Yu.M.Bunkov, M.I.Kurkin, A.P. Tankeev, JETP Lett. **105**, 24 (2017).
[51] A.I. Akhiezer, V.G. Bar'yakhtar, S.V. Peletminskii, *Spin Waves* (North-Holland, Amsterdam, New York, 1968).
[52] E.A. Turov, A.V. Kolchanov, M.I. Kurkin, I.F. Mirsaev, V.V. Nikolaev, *Symmetry and physical properties of antiferromagnetics* (CISP - Cambridge Int. Science Publishing, 2010).
[53] E.A. Turov, M.I. Kurkin, V.V. Nikolaev, Sov. Phys. JETP **37**, 147 (1973).
[54] S.V. Tyablikov, *Methods in the Quantum Theory of Magnetism* (Springer, 2013).
[55] S.V. Vonosovskii, *Magnetism* (Wiley, New York, 1974).
[56] E. A. Turov, V. G. Kuleev, Sov. Phys. JETP **22**, 176 (1966).
[57] A. Abragam, *The Principles of Nuclear Magnetism* (Oxford University Press, New Your, 1961).
[58] W. N. Hardy and L. A. Whitehead, Rev. Sci. Instrum. **52**, 213 (1981).
[59] L.V. Abdurakhimov, Yu.M. Bunkov, D. Konstantinov, Phys. Rev. Lett. **114**, 226402 (2015).
[60] V. A. Tulin, Sov. Phys. JETP **78**, 149 (1980).
[61] M.I. Kurkin, Yu.G. Raidugin, V.N. Sedyshkin, A.P. Tankeev, Sov. Phys. Sol. State **32**, 923 (1990).